Dynamics and stability of moving fronts of water evaporation in a porous medium

Vladimir A. Shargatov[1], Andrej T. Il'ichev[2,3] and George G. Tsypkin[4]

[1] National Research Nuclear University "MePHI", Kashirskoye shosse 31, 115409 Moscow, Russia

[2]Steklov Mathematical Institute, Russian Ac. Sci., Gubkina Str. 8, 119991 Moscow, Russia

[3] Bauman Moscow Technical University, Baumanskaya str. 5, 105110 Moscow, Russia

[4]Institute for Problems in Mechanics, Russian Ac. Sci., Vernadskogo pr., 101 119526 Moscow , Russia

Abstract

We study stability of non-steady plane water evaporation fronts, arising in vertical flows with phase transition in horizontally extended domains of a porous medium. Isothermal motions in the non-wettable horizontal porous medium when a water layer is located over a vapor one is considered and homogeneous capillary forces on the phase transition front are taken into consideration. It is shown that motion of the mobile phase transition fronts depend on their initial position relative to bifurcation curves of the stationary fronts. The four domains in the parameter space are picked out where behavior of linear perturbations of the mobile fronts are different: in the first domain all perturbations decrease, in the second one only long-wave perturbations grow, in the third domain only short-wave perturbations grow and in the fourth one all perturbations grow. Dynamics of localized finite amplitude perturbations of the moving phase transition front are also studied numerically. It is established that their evolution is mainly influenced by the initial position of the perturbed front relative to the mentioned stability/instability domains.

Keywords: porous medium, phase transition front, evaporation, stability

1 Introduction

We consider the model describing, for example, filtration processes in natural massifs, having contact with mines, tunnels and other constructions. The functioning of such engineering systems is accompanied by heat and mass exchange between the construction and surrounding rock [1]. Artificial ventilation makes it possible to keep the micro-climate,

necessary for exploitation. Ventilation is accompanied by evaporation from a ceiling of the construction while the ground water moves downwards under the action of gravity or pressure in the water horizon. The water can enter the underground construction either in liquid or vapor states. If the surrounding rock has relatively low permeability it is natural to assume that the underground water moving towards the ceiling of the construction evaporates somewhere in a porous space and diffuses into the underground construction as a vapor. In this case a region saturated with a blend of vapor and air arises between the free space and water saturated region.

It is well known that for immiscible fluids the configuration with the heavier fluid overlying the lighter one is always subjected to the Rayleigh-Taylor instability even in a porous medium having an arbitrary small permeability [2]. The interface separating immiscible fluids has to deform in a way to prevent both fluids from blending, rather than the phase transition front, which deformations keep the temperature and pressure values for it on the Clapeyron curve of phase equilibrium. This difference in physical properties of the interface and the phase transition front explains the possibility of existence of a stable configuration with phase transitions even in the case when the heavier fluid overlies the lighter one in the porous medium. For the first time the stability of such a configuration was considered in [2] (see also [3, 4, 5]) where an example of a geothermal system is treated and existence of two domains saturated by motionless water and vapor is supposed.

As it was mentioned, in the case under consideration, the domain is formed saturated with a blend of vapor and air and located under the water saturated domain. The arising stationary evaporation front separating these two domains can be either stable or non-stable [6, 7]. In [6] by the method of normal forms stability of the vertical flow was studied with the stationary phase transition front. This stability analysis concerns the behavior of infinitely small harmonic perturbations of the front. It was shown that there exist two types of instability. The first one is newly found and implies first destabilization of the mode with zero wave number (long-wave instability), and the second implies first destabilization of the mode with infinite wave number (short-wave instability). Analysis when the basic regime with the stationary plane phase transition front is subjected to finite localized perturbations requires the use of sophisticated numerical methods and along with the study of the basic physical effects allows to determine the bounds of application of fundamental physical results of [6] for the case of localized finite amplitude perturbations [8]. In [6, 7] it is also shown that a narrow band of weakly unstable modes in some neighborhood of the instability threshold of the existing pair of phase transition fronts are described by the nonlinear diffusion KPP equation [9]. All studies were done for the case of a non-wettable rock.

In this paper we consider stability properties of moving phase transition fronts and the dynamics of their linear and nonlinear perturbations in the described system. The paper is organized as follows. In Sec. 2 we give the formulation of the problem. The

forms of the solutions describing the vertical flow with stationary and moving front are given in Sec. 3. Section 4 is devoted to linear stability analysis of the stationary and moving fronts of phase transition. In Sec. 5 we consider dynamics of nonlinear localized disturbances of the moving fronts. In Sec. 6 we present our conclusion and discussion.

2 Formulation

Nomenclature

Latin symbols

a	[m^2 s^{-1}]	thermal diffusivity
q	[J kg^{-1}]	specific heat of phase transition
$\mathbf{w}$	[m s^{-1}]	velocity
$\mathbf{n}$	[m]	vector of normal
g	[m s^{-2}]	acceleration of gravity
h	[m]	location parameter of the interface
k	[m^2]	permeability
L	[m]	thickness of the low permeable stratum
m	[1]	porosity
P	[Pa]	pressure
D	[m^2 s^{-1}]	diffusion coefficient
t	[s]	time
T	[K]	temperature
$\mathbf{V}$	[m s^{-1}]	velocity of the phase transition interface
R	[J kg^{-1} K^{-1}]	Clapeyron constant
z	[m]	vertical coordinate
$Z(t)$	[m]	location of the moving phase transition front
x	[m]	horizontal coordinate

Greek symbols

ν	[1]	humidity
η	[m]	perturbation of the interface
$\varkappa$	[m^{-1}]	wave number
κ	[1]	dimensionless exponent for nonhomogeneous perturbations
λ	[W m^{-1} K]	thermal conductivity
μ	[Pa s]	viscosity
ρ	[kg m^{-3}]	density
σ	[s^{-1}]	spectral parameter

Subscripts

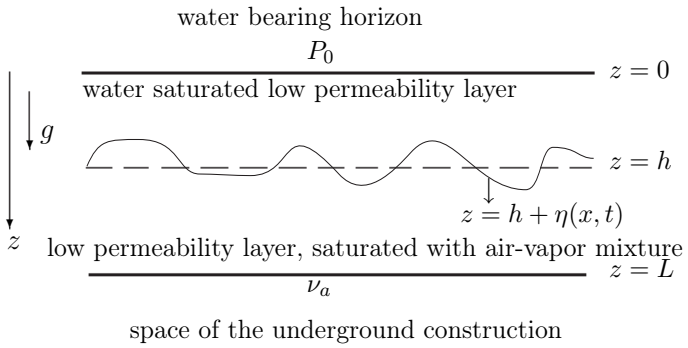

Figure 1: Schematic of the system considered; see the text for explanations.

1	right ahead of the interface in the water saturated domain
2	right behind the interface in the vapour domain
n	normal
D	diffusion
v	vapour
w	water
a	air
c	capillary
0	boundary value at $z = 0$
$*$	at the phase transition front

Superscript

0	boundary value at $z = L$
$'$	perturbation

Let the high permeability water horizon with the water pressure P_0, bounded from below by the plane $z = 0$, be located over the ceiling $z = L$ (the z-axis is directed downwards). The rock in a layer $0 < z < L$ has a low permeability and at the surface $z = L$ it is streamlined by the air of humidity ν_a which is smaller than the humidity of saturation, i. e. the partial pressure in the air is smaller than the pressure of saturation of the vapor in the air at a given value of temperature T. In this case the low permeability porous media $0 < z < L$ contains the water layer $0 < z < h$ and the layer $h < z < L$, saturated by a blend of the air and the water vapor (Fig. 1). **The horizontal coordinate varying from $-\infty$ to ∞ is denoted by x.**

We assume that there exists the front where the evaporation occurs located between the water saturated domain and the domain containing the homogeneous blend of the air and the vapor. Then, in the domain filled in by the liquid phase the inflow of the water from the high permeability horizon takes place towards the front of evaporation. The vapor arising at the front diffuses through the air-vapor domain in the direction

of free surface $z = L$ (the ceiling of the underground construction) streamlined by the air. The vapor diffusion occurs in the case when the partial pressure of the vapor in the neighborhood of the evaporation front is greater than the partial pressure at the free surface $z = L$.

Assuming the water to be incompressible we get the continuity equation and Darcy's law constituting the governing equations in the water saturated domain

$$\text{div } \mathbf{w}_w = 0, \qquad m\mathbf{w}_w = -\frac{k}{\mu_w} \text{ grad } (P - \rho_w g z). \tag{2.1}$$

The governing equations in the domain saturated by the air-vapor blend represent the equation of the vapor diffusion and the Clapeyron equations for gases:

$$\frac{\partial \rho_v}{\partial t} = \text{div}\big(D \,\text{grad}\, \rho_v\big), \quad P_v = \rho_v R_v T, \quad P_a = \rho_a R_a T. \tag{2.2}$$

Here $\mathbf{w}$ is the velocity, m is the porosity, k is the permeability, μ is the viscosity, P is the pressure, g is the gravity, ρ is the density, T is the temperature and D is the diffusion coefficient. Typical values are (see e. g. [10]) $D = 2.4 \times 10^{-5}$ m^{2}s^{-1}, $P_a = 10^5$ Pa, $R_a = 287$ J kg^{-1}K^{-1}, $R_v = 461$ J kg^{-1}K^{-1}. The subscripts v, w and a correspond to the vapor, the water and the air, respectively.

Instead of the equation for the vapor density it is convenient to use the equation for the humidity function $\nu = \rho_v/(\rho_a + \rho_v)$. This equation follows from $(2.2)_1$ under the condition of smallness of the partial pressure of the vapor in comparison with the atmospheric pressure [10]:

$$\frac{\partial \nu}{\partial t} = D \, \Delta \nu. \tag{2.3}$$

The temperature fields T in both domains of the low-permeability medium are governed by the equations (see e. g. [4])

$$\frac{\partial T_{w,v}}{\partial t} = a \Delta T_{w,v}, \tag{2.4}$$

where a is the thermal diffusivity of the surrounding rock.

Considering the stability of the front we notice that the process of the water evaporation is slow and as a consequence the influence of the heat absorbtion during evaporation is negligible. We treat the isothermal problem when the temperature of surrounding rocks T is equal to that one of the ventilated air. This makes it possible to eliminate from the analysis the temperature field and to reduce the problem to the purely hydrodynamic one.

The above conclusions are supported by the following estimates. On the phase transition front the following conditions are fulfilled:

• the conservation of **mass**

$$\rho_w\big((\mathbf{w}_w)_n - \mathbf{V}_n\big) = \rho_v\big((\mathbf{w}_v)_n - \mathbf{V}_n\big), \tag{2.5}$$

where $(\mathbf{w}_w)_n$ is the normal velocity of the water flow through the front,

$$\rho_v(\mathbf{w}_v)_n = -\rho_a(D\,\mathrm{grad}\,\nu)_n, \tag{2.6}$$

is the normal component of diffusive flux of the vapor, and $\mathbf{V}_n$ the normal component of the speed of the phase transition front;

• the condition of the balance of heat

$$\lambda\big(\mathrm{grad}\,T_v - \mathrm{grad}\,T_w\big)\cdot\mathbf{n} = mq\rho_w\big((\mathbf{w}_w)_n - \mathbf{V}_n\big), \tag{2.7}$$

where λ is the coefficient of the thermal conductivity of the porous media, and q is the latent heat.

The typical values of physical quantities in (2.5), (2.7) at $T = 293$ K are (see, e. g. [10])

$$\rho_a = 1.2\,\mathrm{kg}\cdot\mathrm{m}^{-3},\ 0.008\,\mathrm{kg}\cdot\mathrm{m}^{-3} \le \rho_v \le 0.017\,\mathrm{kg}\cdot\mathrm{m}^{-3},\ q = 2.04\times10^6\,\mathrm{J}\cdot\mathrm{kg}^{-1},$$
$$\lambda = 1\,\mathrm{W}\cdot\mathrm{K}^{-1}\cdot\mathrm{m}^{-2},\ m = 0.25.$$

As it follows from equations (2.3) and (2.4) the characteristic length scales, L_ν and L_T, over which the humidity and temperature fields vary are [11]

$$L_\nu \sim \sqrt{D\ t}, \quad L_T \sim \sqrt{a\ t}, \tag{2.8}$$

where the thermal diffusivity $a \sim 10^{-6}$ m^2 s^{-1}.

The ratio ρ_v/ρ_w is very small, hence from (2.5) and (2.7) it easily follows the Stefan condition at the phase transition front

$$\lambda\big(\mathrm{grad}\,T_w - \mathrm{grad}\,T_v\big)\cdot\mathbf{n} = mq\rho_w(\mathbf{w}_D)_n, \tag{2.9}$$

where $\mathbf{w}_D$ is given by

$$\mathbf{w}_D = -\frac{\rho_a}{\rho_w}(D\,\mathrm{grad}\,\nu). \tag{2.10}$$

From (2.9) and (2.10) the following estimate can be obtained

$$\lambda\frac{|\delta T|}{L_T} \sim m\ \rho_w\ q\ D\frac{\rho_a}{\rho_w}\frac{|\delta\nu|}{L_\nu}, \tag{2.11}$$

where $\delta\,T$ is the characteristic variation of the temperature, and $\delta\nu$ is the characteristic variation of the humidity. From (2.11) and using (2.8) we have

$$|\delta T| \sim \frac{m\ \rho_a\ q}{\lambda}\ \sqrt{aD}\ |\delta\nu|. \tag{2.12}$$

Substituting in (2.12) typical values of the parameters we get

$$|\delta T| < 0.25\cdot1.2\cdot2\cdot10^6\ \sqrt{10^{-6}\cdot2.4\cdot10^{-5}}\ 1.7\cdot10^{-2}\,\mathrm{K} < 5\cdot10^{-2}\,\mathrm{K}.$$

Thus, the estimate gives insignificant variation in temperature $|\delta T| < 0.05$ K due to the evaporation process.

The system of equations (2.1) in the water domain is reduced to the Laplace equation

$$\Delta\, P = 0. \tag{2.13}$$

To determine the boundary conditions at the front we assume that the full pressure in the domain of the air-vapor blend coincides with the pressure in a free space of the underground construction and equals to the atmospheric one. It means that there is no gas filtration in the air-vapor domain. On the phase transition front $z = h + \eta(x,t)$ the difference between the pressure in the water domain and that one in the gas domain depends on the physical properties of the surrounding rock and it equals to the capillary pressure. The boundary condition at the front for a pressure jump reads

$$P_w = P_v + P_c \equiv P_a + P_c. \tag{2.14}$$

Here the capillary pressure P_c is negative, when the rock is wettable and it is positive for the non-wettable rock. The boundary condition for the humidity at the front follows from the definition of the humidity function and Clapeyron's equations for the air and vapor:

$$\nu = \nu_* = \frac{R_a}{R_v}\frac{P_{v*}}{P_a}. \tag{2.15}$$

The dependence of the partial pressure on the temperature can be presented as follows [12]

$$P_v = F(T) \qquad \text{or} \qquad \nu_* = \frac{R_a}{R_v}\frac{F(T)}{P_a},$$

$$F(T) = 10^5 \exp\left[-7226.6\left(\frac{1}{T} - \frac{1}{373.16}\right) + 8.2\ln\frac{373.16}{T} - 0.0057(373.16 - T)\right].$$

From the assumption that the processes under consideration are isothermal it follows that the humidity on the front being a function of the temperature is a constant in the framework of our model. The water **mass** conservation law (2.5) with the use of (2.6) and Darcy's law in (2.1) at the front takes the form

$$\left(1 - \frac{\rho_v}{\rho_w}\right)\mathbf{V}_n = -\frac{k}{m\mu_w}\left[\ \text{grad}\ (P - \rho_w g z)\right]_n + D\frac{\rho_a}{\rho_w}\left(\ \text{grad}\ \nu\right)_n. \tag{2.16}$$

The boundary condition at the upper boundary $z = 0$ and at the lower boundary, coinciding with the ceiling are written as

$$z = 0: \quad P = P_0; \quad z = L: \quad \nu = \nu_a. \tag{2.17}$$

The processes under consideration are characterized by the physical parameters which determine the dimensionless quantities

$$\alpha = \frac{P_c + P_a - P_0}{\rho_w g L}, \qquad \beta = \frac{D}{k}\frac{\rho_a}{\rho_w}(\nu_* - \nu_a)\frac{m\mu_w}{\rho_w g L}, \tag{2.18}$$

playing the considerable role in further observations. We note, that the parameter α in (2.18) is the measure of deviation of the pressure P_0 in the aquifer from the hydrostatic one for the given value of the capillary pressure, and the parameter β characterizes the ratio between the rate of the diffusion transfer of the vapor and the rate of the water flux, caused by the hydrostatic pressure.

For example, for the following values of the physical dimension parameters:

$$P_0 = 2 \cdot 10^5\,\mathrm{Pa},\ P_c = 1.06 \cdot 10^5\,\mathrm{Pa},\ L = 20\,\mathrm{m}$$

the dimensionless $\alpha = 0.03$**. Correspondingly, if**

$$m = 0.15,\ \rho_v = 0.015\,\mathrm{kg}\cdot\mathrm{m}^{-3},\ k = 0.6 \cdot 10^{-17}\,\mathrm{m}^2$$

the dimensionless $\beta = 0.1$**.**

3 Base flow

3.1 Stationary front of phase transition

For given values of the parameters the plane stationary phase transition front locates at some equilibrium position $z = h$. This location is determined as the solution of the stationary problem (2.3), (2.13):

$$\frac{\mathrm{d}^2 P(z)}{\mathrm{d}z^2} = 0, \qquad \frac{\mathrm{d}^2 \nu(z)}{\mathrm{d}z^2} = 0.$$

The conservation of momentum on the front $z = h$ takes the form (see (2.16))

$$\frac{k}{m\mu_w}\left[\left(\frac{\mathrm{d}P}{\mathrm{d}z}\right)_1 - \rho_w g\right] = D\frac{\rho_a}{\rho_w}\left(\frac{\mathrm{d}\nu}{\mathrm{d}z}\right)_2. \tag{3.1}$$

From (2.14), (2.15), (2.17) and (3.1) the expressions for the distribution of pressure and humidity in the layers $0 < z < h$ and $h < z < L$ follow:

$$P_{st} = P_0 + \frac{P_a + P_c - P_0}{h}\,z, \qquad \nu_{st} = \frac{\nu_a - \nu_*}{L - h}\,z + \frac{L\nu_* - h\nu_a}{L - h}, \tag{3.2}$$

and also the equation for the location of the evaporation front:

$$\frac{\alpha}{H} - 1 + \frac{\beta}{1 - H} = 0, \quad H = \frac{h}{L}. \tag{3.3}$$

The quadratic equation (3.3) has the roots

$$H_{s,u} = -\frac{1}{2}\left(\beta - \alpha - 1\right) \pm \frac{1}{2}\sqrt{\left(\beta - \alpha - 1\right)^2 - 4\alpha}, \quad H_s \geq H_u. \tag{3.4}$$

It can be easily seen that for the neutral ($P_c = 0$) or the wettable ($P_c < 0$) porous media, when $\alpha < 0$, one root of (3.4) is positive, and the other is negative. The physical sense has only positive root, corresponding to the sign "+" at the radical in (3.4).

For the non-wettable media for $P_c > 0$ the smallest root can become positive, when the pressure P_0 at the aquifer decreases in a way that α becomes positive. For the further decrease of P_0 the parameter α attains the critical value

$$\beta = \left(1 - \sqrt{\alpha}\right)^2.$$

At this value the coincidence of the roots of (3.4) takes place, and the stationary solution (3.2) ceases to exist, when α exceeds this critical value [6].

The solution (3.2) describes the stationary process of evaporation on the phase transition front when the heavier fluid (water) is located above the lighter one (air-vapor blend). In the case when there exists the unique location for the stationary front of phase transition it is stable and it is evident that this solution describes the penetration of the moisture in the underground construction as a result of the vapor diffusion through the rock. If two locations of equilibrium positions of the phase transition front are possible, i. e. the both roots of (3.3) are positive, one of them is always dynamically unstable (see subsection 4.1).

3.2 Moving front of phase transition

If the phase transition front is plane at the moment t and any point of it has the coordinate $z = Z(t)$, then the distribution of pressure in the layer $0 < z < Z(t)$ depends on time and vertical coordinate z, and it follows from (2.13) that

$$P_{st}(z) = P_0 + \frac{(P_a + P_c - P_0)z}{Z(t)}. \tag{3.5}$$

With the use of (3.5) the problem (2.3), (2.15), (2.16) and (2.17) can be written as (neglecting the small ratio ρ_v/ρ_w)

$$D\,\frac{\partial^2}{\partial z^2}\nu\,(z,t\,) = \frac{\partial}{\partial t}\nu\,(z,t\,), \qquad \nu\,(L,t\,) = \nu_a, \qquad \nu\,\big(Z\,(t\,),t\,\big) = \nu_*,$$
$$Z\,(0\,){=}Z_0,\ \frac{dZ\,(t\,)}{dt} = -\,\frac{k\,(P_a + P_c - P_0\,)}{m\mu_w Z\,(t\,)} + \frac{D\rho_a\big(\frac{\partial}{\partial z}\nu(z,t)\big)|_{z=Z(t)}}{\rho_w} + \frac{k\rho_w g}{m\mu_w}. \tag{3.6}$$

Introduce dimensionless variables

$$\tau = \frac{tm\mu_w}{Lk\rho_w g}, \quad \zeta = \frac{z}{L}, \quad \overline{Z}(\tau) = \frac{Z\,(t\,)}{L}, \quad \overline{\nu}\,(\zeta,\tau\,) = \frac{\nu\,(z,t\,) - \nu_a}{\nu_* - \nu_a}.$$

In these variables (3.6) is written as

$$\beta\,G\frac{\partial^2}{\partial\zeta^2}\overline{\nu}\,(\zeta,\tau\,) = \frac{\partial}{\partial\tau}\overline{\nu}\,(\zeta,\tau\,), \quad \overline{\nu}\big(\overline{Z}\,(\tau\,),\tau\,\big) = 1, \quad \overline{\nu}\,(1,\tau\,) = 0,$$
$$\overline{Z}(0\,) = \overline{Z}_0, \quad \frac{d}{d\tau}\overline{Z}\,(\tau\,) = -\frac{\alpha}{\overline{Z}\,(\tau\,)} + \beta\,\frac{\partial}{\partial\zeta}\overline{\nu}\,(\zeta,\tau\,) + 1, \tag{3.7}$$

where

$$G = \frac{\rho_w}{(\nu_* - \nu_a\ )\rho_a}.$$

The solution of (3.7) depends on the three dimensionless parameters α, β and G.

The stationary analogue of (3.7) is given by

$$\frac{\partial^2}{\partial\zeta^2}\overline{\nu}\ (\zeta, \tau\ ) = 0, \qquad \overline{\nu}\ \left(\overline{Z}_s\ (\tau\ ), \tau\ \right) = 1, \qquad \overline{\nu}\ (1, \tau\ ) = 0. \tag{3.8}$$

The corresponding solution of (3.8) has the form

$$\overline{\nu}_s\,(\zeta, \tau) = 1 - \frac{\zeta - \overline{Z}_s\,(\tau)}{1 - \overline{Z}_s\,(\tau)} \tag{3.9}$$

The characteristic time of asymptotic approach of the solution of (3.7) to (3.9) equals to $\tau_{as} \sim 1/(\beta\, G)$.

The characteristic time of **diffusion** is determined by the absolute value of the **diffusion** rate (2.10)

$$t_D \sim \frac{L - h}{|\mathbf{w}_D|},$$

or

$$t_D \sim \frac{(L - h)\rho_w}{D\rho_a \frac{|\partial\nu|}{|\partial z|}}. \tag{3.10}$$

In dimensionless form (3.10) reads

$$\tau_D < |\beta\frac{\partial}{\partial\zeta}\overline{\nu}\ (\zeta, \tau\ )|^{\ -1}.$$

Provided $\frac{\partial}{\partial\zeta}\overline{\nu}\ (\zeta, \tau\ ) \sim 1$, we have

$$\frac{\tau_{as}}{\tau_D} \sim \frac{1}{G} \ll 1. \tag{3.11}$$

It can be seen from (3.11) that evaporation is a slow process in comparison with convergence to stationary distribution (3.9).

These conclusions are confirmed by the results of numeric calculation. The difference between values of $\overline{Z}(\tau)$, computed using stationary and non-stationary diffusion equations did not exceed 0.1%.

For the stationary distribution (3.9) it is possible to get the analytic solution of (3.7). Substitute (3.9) in $(3.7)_5$ to obtain the equation of the phase transition front motion:

$$\frac{d}{d\tau}\overline{Z}_s\ (\tau\ ) = -\frac{\alpha}{\overline{Z}_s\ (\tau\ )} - \frac{\beta}{1 - \overline{Z}_s\ (\tau\ )} + 1$$

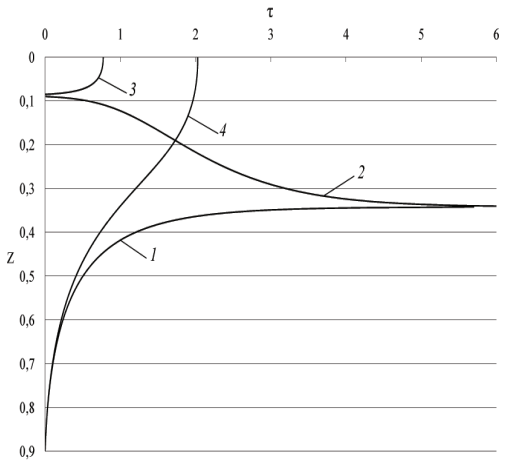

Figure 2: Dependence of the location of the phase transition front on time; $\alpha = 0.03$ $\beta = 0.6$. 1 - $\overline{Z}_0 = 0.9$; 2 - $\overline{Z}_0 = 0.09$; 3 - $\overline{Z}_0 = 0.085$; 4 - $\overline{Z}_0 = 0.9$, $\alpha = 0.1$. The difference between the numerically computed solution and the solution as given by (3.12) is not visible in the picture.

This equation has the analytic solution $\tau(\overline{Z}_s)$. Denote

$$c = (\alpha - \beta + 1)/2, \quad d = ((\alpha - \beta + 1)/2)^2 - \alpha.$$

Then the implicit form of the solution is

$$\begin{aligned}
&\tau = \frac{c^2 - c + d}{\sqrt{-d}} \arctan\left(\frac{\overline{Z}_s - c}{\sqrt{-d}}\right) + (c - 1/2)\ln\left((\overline{Z}_s - c)^2 - d\right) + \overline{Z}_s - \\
&- \frac{c^2 - c + d}{\sqrt{-d}} \arctan\left(\frac{\overline{Z}_0 - c}{\sqrt{-d}}\right) - (c - 1/2)\ln\left((\overline{Z}_0 - c)^2 - d\right) - \overline{Z}_0 \\
&\text{if} \quad d < 0, \\
&\tau = \frac{c^2 - c + d}{\sqrt{d}} \operatorname{arctanh}\left(\frac{\overline{Z}_s - c}{\sqrt{d}}\right) + (c - 1/2)\ln\left((\overline{Z}_s - c)^2 - d\right) + \overline{Z}_s - \\
&- \frac{c^2 - c + d}{\sqrt{d}} \operatorname{arctanh}\left(\frac{\overline{Z}_0 - c}{\sqrt{d}}\right) - (c - 1/2)\ln\left((\overline{Z}_0 - c)^2 - d\right) - \overline{Z}_0, \\
&\text{if} \quad d > 0.
\end{aligned} \tag{3.12}$$

If $d < 0$ the stationary solution for the standing plane phase transition front does not exist (see (3.4)).

In Fig. 2 we show all possible types of the behavior of $\overline{Z}$ (τ). Lines 1-3 are plotted for the values $\alpha = 0.03$ and $\beta = 0.6$. In this case for $\overline{Z} = 0.342$ there exists the stable front, and for $\overline{Z} = 0.0876$ – unstable. Line 1 is plotted for the initial value $\overline{Z}_0 = 0.9$. At the initial moment the front is located under the equilibrium position and it tends asymptotically to it. Line 2 corresponds to $\overline{Z}_0 = 0.09$. At the initial moment front is located above the stable equilibrium position, but under unstable equilibrium position and asymptotically tends to the stable equilibrium position from above. Line 3 corresponds to

$\overline{Z}_0 = 0.085$. At the initial moment the front is located above the unstable equilibrium position. It moves upwards and for finite time attains the position $z = 0$. Line 4 corresponds to $\overline{Z}_0 = 0.9$ and $\alpha = 0.1$. The positions of equilibrium of the phase transition front are absent for $\alpha = 0.1$ and $\beta = 0.6$. As in the latter case the front begins to move upwards becoming slower, then it accelerates and for finite time attains the upper boundary of the layer $z = 0$. The results of numeric computation differs by the computation according to (3.12) in a way not visible in the figure.

4 Stability

4.1 Stationary phase transition fronts

Destabilization of the basic regime is possible only in the case of the non-wettable porous media ($\alpha > 0$). Consequently, we consider only this case. The equations (2.3) and (2.13) are linear, therefore, we linearize only the boundary conditions about the solution (3.2). Let P', ν', η be the perturbations of the basic pressure, humidity and variation of the location of phase transition front, correspondingly. The linearized form of the conservation law (2.16) has the form

$$\frac{\partial \eta}{\partial t} = -\frac{k}{m\mu_w}\left(\frac{\partial P'}{\partial z}\right)_1 + D\frac{\rho_a}{\rho_w}\left(\frac{\partial \nu'}{\partial z}\right)_2. \tag{4.1}$$

The condition of the jump of pressure (2.14) and that one of the constancy of humidity (2.15) on the front are given by

$$P' + \frac{dP_{st}}{dz}\eta = 0, \qquad \nu' + \frac{d\nu_{st}}{dz}\eta = 0, \qquad z(t,x) = h. \tag{4.2}$$

We look for the solution of (4.1), (4.2) in the form $\{P', \nu', \eta\} = \{\hat{P}(z), \hat{\nu}(z), \hat{\eta}\}\exp(\sigma t + i\varkappa x)$. The expressions for the amplitudes are given by

$$\hat{P}(z) = \hat{P}_- \frac{\operatorname{sh}\varkappa z}{\operatorname{sh}\varkappa h},$$

$$\hat{\nu}(z) = \hat{\nu}_+ \frac{\operatorname{sh} e(L-z)}{\operatorname{sh} e(L-h)},$$

where $e^2 = \sigma/D + \varkappa^2$.

Put $K = \varkappa L$, $\Sigma = \sigma L^2/D$. We consider the mechanism of destabilization satisfying the principle of exchange of stabilities, i. e. when Σ equals zero on the threshold of stability. In [6] it is shown that the equation of the marginal set $\Sigma = 0$ has the form

$$f(K) \equiv \frac{\coth K(1-H)}{\coth KH} = \frac{\alpha}{\beta}\,\frac{1-H}{H} \equiv \Delta. \tag{4.3}$$

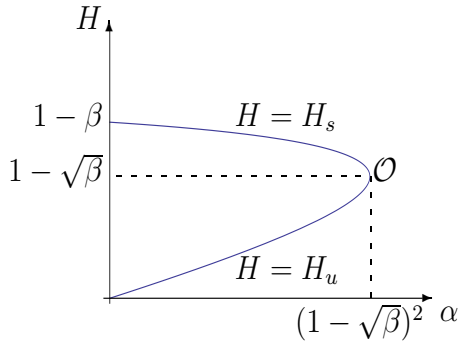

Figure 3: Bifurcation diagram H versus α at a fixed β in (2.18); $H = H_s$ is the stable branch, $H = H_u$ the unstable branch, $\mathcal{O}$ is the turning point.

It was found [6] that if the values of the left hand side of the equation (4.3) for some K are less than the value of the right hand side then the base solution is unstable, i. e. $\Sigma > 0$ for these K.

It can be found that there exist two scenarios of transition to instability. The first one was invented for the first time in [6] and it corresponds to the first destabilization of the mode with $K = 0$ (long-wave instability). It was established [6], that in a neighborhood of the threshold of instability for the transition through $K = 0$ there exist exactly two vertical flows, corresponding to the different locations of phase transition fronts. One of these fronts is stable and the other is unstable. At the threshold of instability of the stable front the coincidence of both fronts takes place. The bifurcation diagram was shown in Fig. 3. The diagram is typical for the classical turning point bifurcation where one branch is stable and the other is unstable. The solution, corresponding to the stable branch (branch $H = H_s$), is impossible to continue through the turning point $\mathcal{O}$ where it looses its stability.

The other destabilization corresponds to the first destabilization of the mode with $K = \infty$ (short-wave instability). The short-wave instability, apparently, has an artificial character and may be excluded from the treatment of the model. One of the conjectures why it takes place is the fact that for extremely short waves the interface between the water and the vapor is impossible to consider as the sharp interface between this two phases. Like the stratified fluids with a shift of speeds, when always presents the short-wave Kelvin-Helmholtz instability, the contact interface has to be treated as the zone of the blend of two fluids [13]. The domains of stability *St*, long-wave instability *Lo*, short-wave instability *S* and both long-short wave instability *U* in the $(r = \alpha/\beta, H)$-plane are shown in Fig. 4.

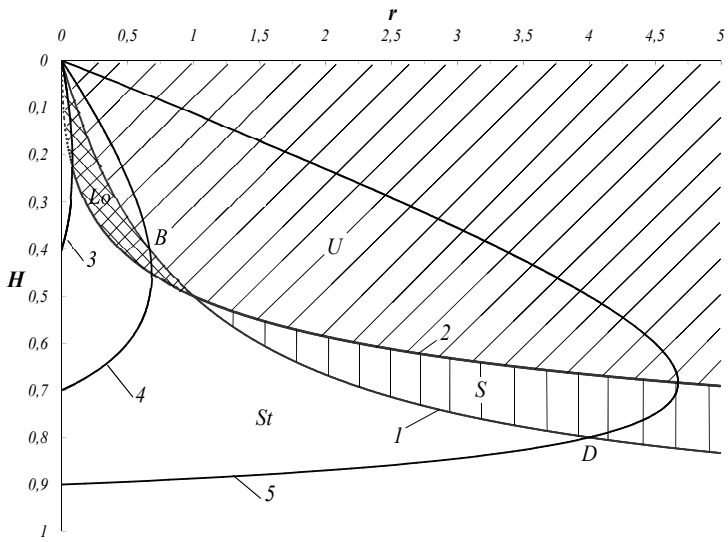

Figure 4: The domains of stability *St*, long wave instability *Lo*, short wave instability *S* and both long-short wave instability *U* in the $(r=\alpha/\beta, H)$-plane; 1 – $H=r/(1+r)$; 2 - $H=\sqrt{r}/(1+\sqrt{r})$. Bifurcation diagrams (dependence of H on r for fixed β) : 3 - $\beta=0.6$, 4 -$\beta=0.3$, 5 - $\beta=0.1$.

4.2 Moving front of phase transition

According to the results of the subsection 3.2 we consider the problem in the "quasi-stationary" approximation:

$$\left(\frac{\partial^2}{\partial\zeta^2}\overline{P}\ (\chi,\zeta,\tau\ )+\frac{\partial^2}{\partial\chi^2}\overline{P}\ (\chi,\zeta,\tau\ )\right)=0,\quad \overline{P}\ (\chi,\overline{h}\ (\chi,\tau\ ),\tau\ )=1,\quad \overline{P}\ (\chi,0,\tau\ )=0,$$
$$\beta\,G\left(\frac{\partial^2}{\partial\zeta^2}\overline{\nu}\ (\chi,\zeta,\tau\ )+\frac{\partial^2}{\partial\chi^2}\overline{\nu}\ (\chi,\zeta,\tau\ )\right)=0,\quad \overline{\nu}\ (\chi,\overline{h}\ (\chi,\tau\ ),\tau\ )=1,\quad \overline{\nu}\ (\chi,1,\tau\ )=0,$$
$$\frac{\partial}{\partial\tau}\overline{h}\ (\chi,\tau\ )=-\,\alpha\,\frac{\partial}{\partial\zeta}\overline{P}\ (\chi,\zeta,\tau\ )|_{\zeta=\overline{h}(\chi,\tau\ )}+\beta\,\frac{\partial}{\partial\zeta}\overline{\nu}\ (\chi,\zeta,\tau\ )|_{\zeta=\overline{h}(\chi,\tau\ )}+1,\quad \overline{h}\ (\chi,0\ )=\overline{h}_0, \tag{4.4}$$

where

$$\chi=x/L,\quad \overline{h}=h/L,\quad \overline{P}(\chi,\zeta,\tau)=\frac{P-P_0}{P_a+P_c-P_0}. \tag{4.5}$$

Let

$$\overline{P}\ (\chi,\zeta,\tau\ )=\overline{P}_{st}(\zeta,\tau\ )+P'(\chi,\zeta,\tau\ ),\quad \overline{\nu}\ (\chi,\zeta,\tau\ )=\overline{\nu}_s(\zeta,\tau\ )+\nu'(\chi,\zeta,\tau\ ),$$
$$\overline{h}\ (\chi,\tau\ )=\overline{Z}_s(\tau)+\eta(\chi,\tau\ ), \tag{4.6}$$

where $\overline{P}_{st}$, $\overline{\nu}_s$, $\overline{Z}_a(\tau)$ are given by (3.5), (4.5), (3.9) and (3.12), respectively. We look for the solutions of the linearized equations (4.4) in the form

$$P'(\chi,\zeta,\tau)=\frac{P_+\hat{P}(\zeta)\hat{\eta}(\tau)\mathrm{e}^{i\kappa\chi}}{\overline{Z}_s(\tau)\sinh(\kappa\overline{Z}_s(\tau))},\quad \nu'(\chi,\zeta,\tau)=\frac{\nu_+\hat{\nu}(\zeta)\hat{\eta}(\tau)\mathrm{e}^{i\kappa\chi}}{(1-\overline{Z}_s(\tau))\sinh(\kappa(1-\overline{Z}_s(\tau)))},$$
$$\eta(\zeta,\tau)=\eta_+\hat{\eta}(\tau)e^{i\kappa\chi}, \tag{4.7}$$

where

$$\hat{P}(\zeta)=\sinh(\kappa\zeta),\quad \hat{\nu}(\zeta)=\sinh(\kappa(1-\zeta)),$$

and P_+, ν_+, η_+ are constants.

Substituting (4.6), (4.7) into (4.4) we get the system of linear equations on P_+, ν_+, η_+

$$P_++\eta_+=0,\quad \nu_+-\eta_+=0,$$
$$\eta_+\frac{d}{d\tau}\hat{\eta}(\tau)=-\frac{P_+\alpha\,\kappa\,\hat{\eta}(\tau)\,\coth(\kappa\overline{Z}_s(\tau))}{\overline{Z}_s(\tau)}-\frac{\nu_+\beta\,\kappa\,\hat{\eta}(\tau)\,\coth(\kappa(1-\overline{Z}_s(\tau))}{1-\overline{Z}_s(\tau)},$$

which has nontrivial solutions when

$$\frac{d}{d\tau}\big(\ln\left(\hat{\eta}(\tau)\right)=-\frac{\beta\kappa}{\tanh(\kappa\overline{Z}_s(\tau))\overline{Z}_s(\tau)}\left(\frac{\tanh\left(\kappa\overline{Z}_s(\tau)\right)\overline{Z}_s(\tau)}{\tanh\left(\kappa\left(1-\overline{Z}_s(\tau)\right)\right)\left(1-\overline{Z}_s(\tau)\right)}-\frac{\alpha}{\beta}\right). \tag{4.8}$$

The multiplier $(\beta\kappa/(\overline{Z}_a\tanh\big(\kappa\overline{Z}_a)))\big)$ in the right-hand side is non-negative, therefore the sign in the right hand side is determined by the expression in brackets. When $\alpha\le 0$ (wettable rock), the expression in the brackets is always positive and any small perturbation decreases with time.

For the first summand in the brackets in (4.8) the inequality is valid

$$\frac{\overline{Z}^2}{(1-\overline{Z})^2}\le\ \frac{\tanh\ (\kappa\overline{Z}\ )\overline{Z}}{\tanh\ (\kappa\ (1-\overline{Z}\ )\ )\ (1-\overline{Z}\ )}\le\frac{\overline{Z}}{(1-\overline{Z})},\quad \text{if}\quad \overline{Z}\le\frac{1}{2},$$
$$\frac{\overline{Z}}{(1-\overline{Z})}\le\ \frac{\tanh\ (\kappa\overline{Z}\ )\overline{Z}}{\tanh\ (\kappa\ (1-\overline{Z}\ )\ )\ (1-\overline{Z}\ )}\le\frac{\overline{Z}^2}{(1-\overline{Z})^2},\quad \text{if}\quad \overline{Z}\ge\frac{1}{2}. \tag{4.9}$$

It follows from (4.9) that the inequality

$$\left(\frac{\tanh\left(\kappa\overline{Z}\right)\overline{Z}}{\tanh\left(\kappa\left(1-\overline{Z}\right)\right)\left(1-\overline{Z}\right)}-\frac{\alpha}{\beta}\right)\ge 0 \tag{4.10}$$

holds for any κ if

$$\frac{\overline{Z}^2}{(1-\overline{Z})^2}\ge r\quad\text{and}\quad\overline{Z}\le\frac{1}{2},\quad\text{or}\quad\frac{\overline{Z}}{(1-\overline{Z})}\ge r\quad\text{and}\quad\overline{Z}\ge\frac{1}{2},$$

and it doesn't hold for some κ if

$$\frac{\overline{Z}}{(1-\overline{Z})}<r\quad\text{and}\quad\overline{Z}\le\frac{1}{2}\quad\text{or}\quad\frac{\overline{Z}^2}{(1-\overline{Z})^2}<r\quad\text{and}\quad\overline{Z}\ge\frac{1}{2},$$

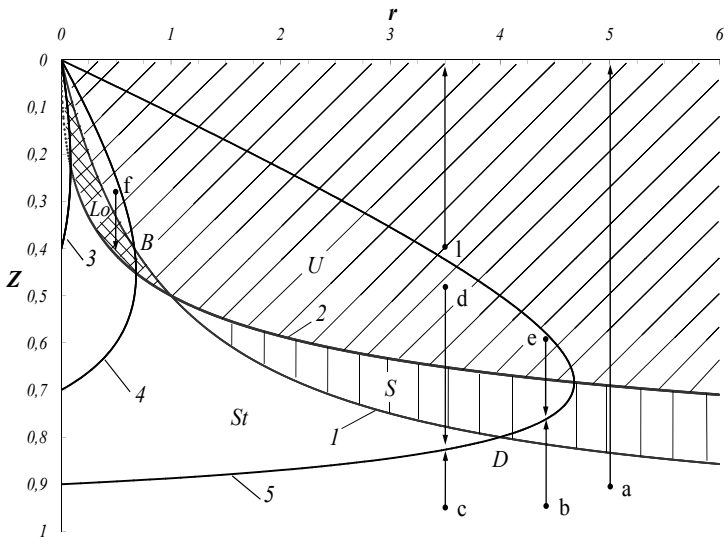

Figure 5: The same as in Fig. 4. The domains St, U, Lo, S are the domains of corresponding behavior of amplitudes of perturbations (see the text). Possible initial position of the front is shown by the Latin letters, tendency of their evolution are shown by arrows.

(we recall, that $r = (\alpha/\beta)$).

The mutual position of the curves

$$r = \frac{\overline{Z}^2}{(1-\overline{Z})^2}, \quad r = \frac{\overline{Z}}{(1-\overline{Z})}$$

is shown in Fig. 5 (the same as curves 1 and 2 in Fig. 4).

In the domain Lo the inequality (4.10) holds for short waves and it doesn't hold for long waves. In the domain S, vise versa, this inequality holds for long waves and doesn't hold for short waves. In the domain St the inequality holds for waves of any length, and in the domain U it doesn't hold at all. Hence, if the front is located in the domain St, an amplitude of any perturbation decreases. If the front is located in the domain U an amplitude of any perturbation grows. In the domain S an amplitude of a short wave perturbation grows, and the amplitude of long-wave perturbation decreases, and vice versa in the domain Lo.

Depending on the initial position and values of r, the front of phase transition either tends to the stable stationary phase transition front (positions $b - f$ in Fig. 5), or at the finite time reaches the upper boundary of the low-permeability layer (initial position a and l in Fig. 5). In this setting, the point in Fig. 5, corresponding to the position of the front moves along the vertical line and can travel from one domain to another. During the time of motion the character of variation of the amplitude of perturbation can change.

The motion of the phase transition front is described by (3.12). Dependence of the amplitude of perturbation on the front coordinate can be got from (4.8):

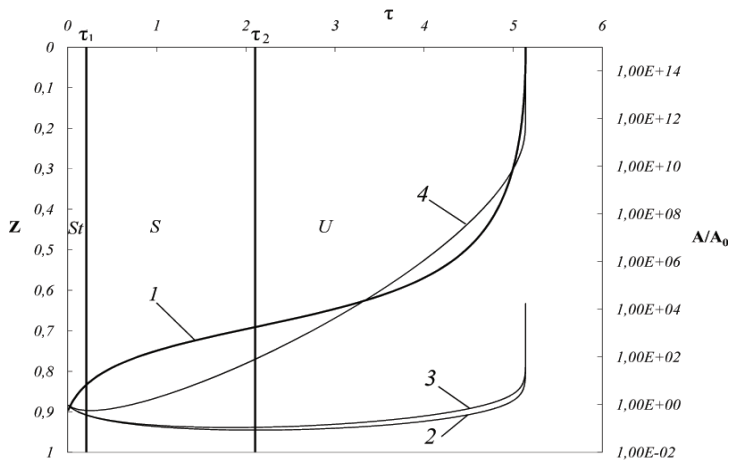

Figure 6: Dependence of the front position $\overline{Z}_s$ (line 1) and the amplitude of perturbation A/A_0 (lines 2, 3, 4; A_0 is the initial and A is the actual amplitudes) on time; $\alpha = 0.5, \beta = 0.1, \overline{Z}_0 = 0.9$: 1 is the position of the front $\overline{Z}_s(\tau)$; 2 is the perturbation with $\kappa = 0.01$; 3 is the perturbation with $\kappa = 1$; 4 is the perturbation with $\kappa = 10$.

$$\hat{\eta}(\overline{Z}_s) = \exp\left[\int_{\overline{Z}_0}^{\overline{Z}_s} \left(\frac{\alpha\,\kappa\,\coth(\kappa\overline{Z})}{\overline{Z}} - \frac{\beta\,\kappa\,\coth(\kappa(1-\overline{Z}))}{1-\overline{Z}}\right)\left(-\frac{\alpha}{\overline{Z}} - \frac{\beta}{1-\overline{Z}} + 1\right)^{-1} d\overline{Z}\right].$$

Dependence of $H(r)$ on three different values of β are shown in Fig. 4 and Fig. 5. This lines illustrate all possible cases of the positions of bifurcation curves $H(r)$ about the domains St , S, Lo and U. The first case: the lower branch of the bifurcation curve can lie entirely in the domain of stability St while the upper branch lies in the domain of long-wave instability Lo (line 3). The second case: the lower branch of the bifurcation curve lies in the domain of stability St while the upper branch lies in the domain of long-wave instability Lo and in the domain of full instability U (line 4). The third case: the lower branch lies in the domain of stability St and in the domain of short-wave instability S while the upper branch lies entirely in the domain of instability U (line 5).

Only solutions, corresponding to the lower branch of the bifurcation curve are stable with respect to long-wave perturbations. In Fig. 5 the lines $a-l$ show possible motions of the front of phase transitions through the domains with different types of instability. The position of the front tends to a point on the lower branch of bifurcation curve, if the initial position locates lower than the upper branch of the bifurcation curve, as it is shown by the lines $b-f$ in Fig 5. If the initial position of the phase transition front locates above the upper equilibrium position or to the right of the turning point, then the front moves to the upper boundary of the low permeability layer as it is shown by the lines a and l in Fig. 5.

We consider the example when the front pases through the different domains of instability in the sequence $St \to S \to U$. Let $\alpha = 0.5$, $\beta = 0.1$, $\overline{Z}_0 = 0.9$. In this case

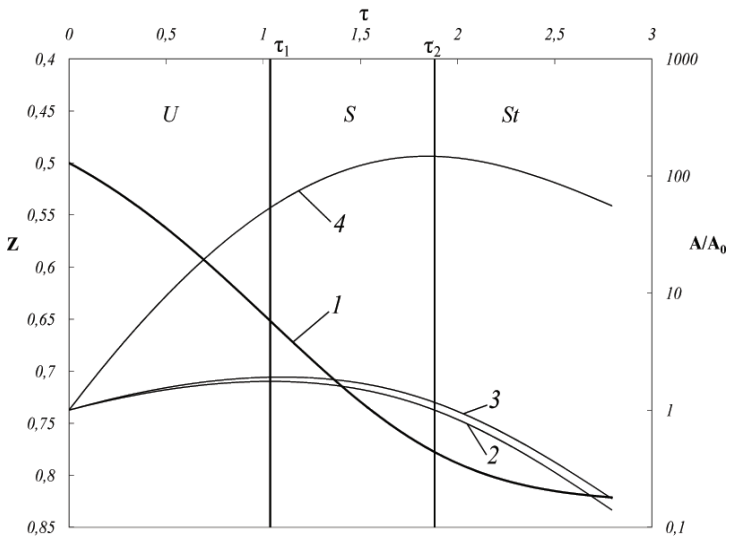

Figure 7: Dependence of the front position $\overline{Z}_s$ (line 1) and the amplitude of perturbation A/A_0 (lines 2, 3, 4) on time; $\alpha = 0.35$, $\beta = 0.1$, $\overline{Z}_0 = 0.5$, 1 is the position of the front $\overline{Z}_s(\tau)$; 2 is the perturbation with $\kappa = 0.01$; 3 is the perturbation with $\kappa = 1$; 4 is the perturbation with $\kappa = 10$.

$r = 5$. The bifurcation diagram for $\beta = 0.1$ is given by the line 5 in Fig. 5, and the initial position of the phase transition front is denoted by the point a. It is seen from Fig. 5 that the turning point lies to the left of the vertical line $r = 5$ and, hence, there are no stationary regimes. As a consequence, the front will move to the upper boundary $z = 0$ of the low-permeability layer as the line a shows. Dependence of the position of the front $\overline{Z}_s$ on time is shown in Fig. 6 by the line 1. In this figure we also show amplitudes of perturbations for various wave-lengths.

When the front is still in the domain St the amplitude of any perturbation decreases. Then the front occurs in the domain S, where one has short-wave instability, therefore first an amplitude of the shortest wave begins to grow (line 4 in Fig. 6). After the entrance in the domain U all wave-lengths are subjected to instability (lines 2, 3, 4, Fig. 6).

Consider the case when the point, corresponding to the initial position of the front locates between the lower and upper branches of the bifurcation curve. In this case the phase transition front moves towards the equilibrium point lying in the stable lower branch of the bifurcation curve. If the initial point lies close to the upper branch, then the front can be initially located either in the domain U, as for the bifurcation shown by the line 5 (lines d, e in Fig. 5), or in the domain Lo. For the scenarios e and d the front passes through the domain U, where all perturbations grow (lines 2, 3, 4 in Figs. 7, 8). Then it gets to the domain S, where long waves damp (lines 2, 3 in Figs. 7, 8), and the amplitude of short waves continues to grow (line 4 in Figs. 7, 8). If the corresponding point on the bifurcation curve lies lower than the domain S, then the front will get to the domain St, where all perturbations damp (lines 2, 3, 4 in Fig. 7). Fig. 8 describes the case, when the

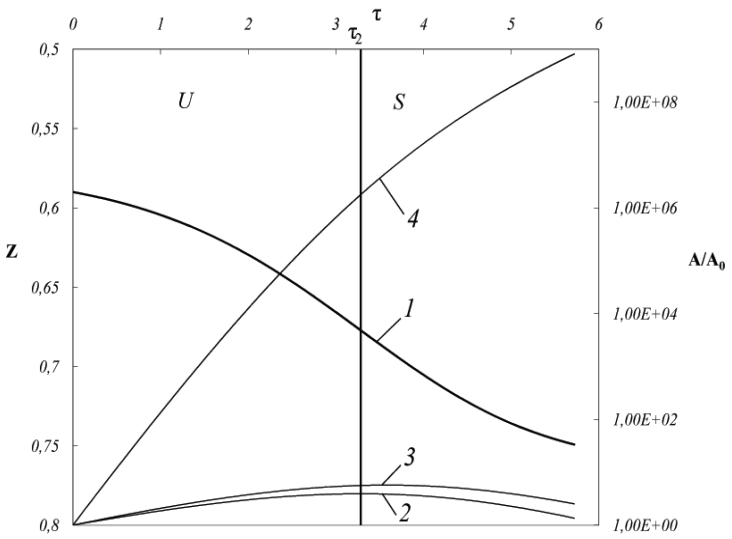

Figure 8: Dependence of the front position $\overline{Z}_s$ (line 1) and amplitude of perturbation A/A_0 (lines 2,3,4) on time; $\alpha = 0.44$, $\beta = 0.1$, $\overline{Z}_0 = 0.59$, 1 is the position of the front $\overline{Z}_s(\tau)$; 2 is the perturbation with $\kappa = 0.01$; 3 is the perturbation with $\kappa = 1$; 4 is the perturbation with $\kappa = 10$.

limiting point on the bifurcation curve lies in the domain S.

5 Evolution of finite localized perturbations of the moving front.

For description of our numerical method we refer to [8]. This method was tested, in particular, by comparison with analytic asymptotic solution, obeying the diffusion KPP equation describing the process when the fronts are located close to each other.

Numeric modeling makes it possible to discover some characteristics of evolution of localized finite perturbations of the moving phase transition front, which dynamics cannot be described by the linear analysis made for infinitesimal harmonic perturbations. Analysis of evolution of infinitesimal harmonic perturbations performed in sec. 4, shows that numeric modeling will meet considerable difficulties in the domains U and S. In these domains short wave instability takes place and the rate of increase of perturbations may be arbitrary large. During the motion of the front the amplitude may grow by several orders (see, e. g. line 4 in Fig. 6). In the domains Lo and St, however, the problem (4.4) can be solved by numerical modeling for sure.

The first calculation is performed when the equilibrium position is absent and initially the front has a location in the domain St ($\alpha = 0.1$, $\beta = 0.6$, $\overline{Z}_0 = 0.4$). The motion takes place according to the scenario $St \to Lo \to U$ to the upper boundary. From Fig. 9

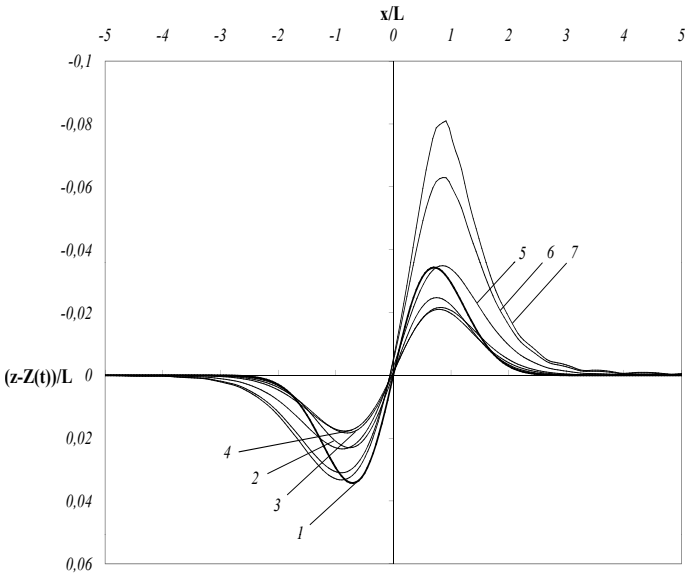

Figure 9: Evolution of the phase transition front when the stationary front doesn't exist; $\alpha = 0.1, \beta = 0.6, \overline{Z}_0 = 0.4$, the curves enumerated in correspondence with growing time.

it is seen, that perturbation evolve according to the scenario of evolution of infinitesimal harmonic perturbations. In the domain St the amplitude of any perturbation decreases (lines 1, 2, 3, 4), then the amplitude begins to grow (lines 5, 6) in the domain Lo, this process accelerates until the maximum of the perturbation reaches the line $z = 0$.

Consider also the case when the front begins to move from the lower boundary of the low-permeability layer and in the process of its motion it finds itself in the domain S of short-wave instability before it reaches the equilibrium at $z = 0.77$ (line b in Fig. 5; $\alpha = 0.44, \beta = 0.1$, $\overline{Z}_0 = 0.95$). The coordinate of the equilibrium position corresponds to the point on that lower branch curve's part which lies in the domain S. Evolution of the plane front of phase transition is shown in Fig. 10. The amplitude of the initial perturbation (line 1) decreases while approaching to the equilibrium point $z = 0.77$ (lines 2,3,4,5). However, short wave disturbances appear and play the dominant role in the front surface evolution after deceleration of the front (line 6).

If the front locates in the domain of long-wave instability Lo, then it dynamics can be modeled numerically, and uncontrolled disturbances are absent. For example, for $\alpha = 0.03$, $\beta = 0.6$, the unstable branch of the bifurcation curve entirely lies in the domain Lo (Fig. 5, line 3). For $\alpha = 0.03$ the unstable equilibrium position locates at $z = 0.0876$, and the stable equilibrium position locates at $z = 0.342$. These equilibrium positions are given in Fig. 11 by lines 7 and 8, correspondingly.

We choose the initial front location $\overline{Z}_0 = 0.125$ between lines 7 and 8 in Fig. 11. This front location corresponds to the scenario $Lo \to St$. The form of the initial perturbation is shown in Fig. 11 by line 1. In this case the character of its evolution qualitatively

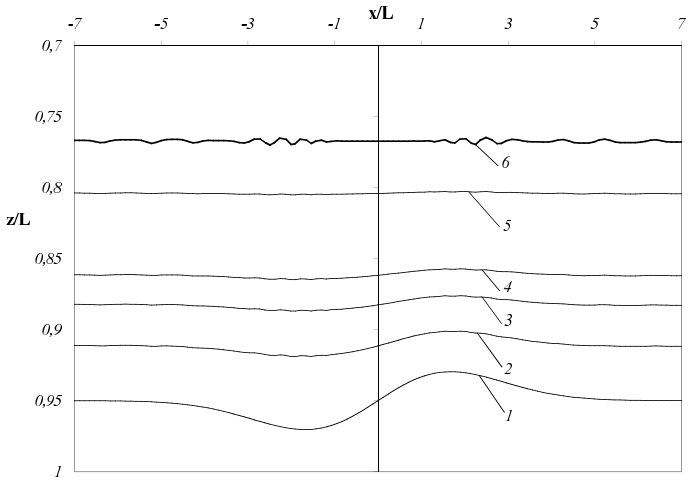

Figure 10: Evolution of the phase transition front for $\alpha = 0.44, \beta = 0.1$, $\overline{Z}_0 = 0.95$ (line b in Fig. 5). The curves enumerated in correspondence with growing time.

corresponds to results for infinitesimal harmonic perturbations. The dependence of the front coordinate on time is shown in Fig. 12. The front moves in the direction of the stable equilibrium, at first the amplitude of perturbations grows (Fig. 12, lines 2 and 3) because the initial "effective" wave-length exceeds the threshold value for long-wave instability, and then decreases as the front tends asymptotically to the stable equilibrium (Fig. 12, lines 2 and 3).

Let us increase then the initial amplitude of the perturbation in such a way that some part of the perturbed front lies above the unstable equilibrium as shown in Fig. 13, line 1. In this case the perturbation directed upstairs begins to grow and the plane part of the front moves downstairs as in the previous case. However, the amplitude of the perturbation grows faster than the plane part of the front moves downstairs. As a result some part of the perturbation of the front (line 4 in Fig. 13) reaches the domain of instability U shown by line 9 in Fig. 13. Note, that the front, as in the previous example, moves according to the scenario $Lo \to St$, but some part of it, containing the maximum of the perturbation directed above, moves in the opposite side and gets from the domain Lo to the domain U.

6 Conclusion and Discussion

We considered here dynamics and stability properties of the moving fronts of phase transition which may arise in vertical flows with phase transition in horizontally extended domains of the porous medium where the water layer is located above the vapor one. The processes are considered to be isothermal, the possibility of this for the problem in question is justified in the sec. 2 of the present paper. We find out that dynamics behavior

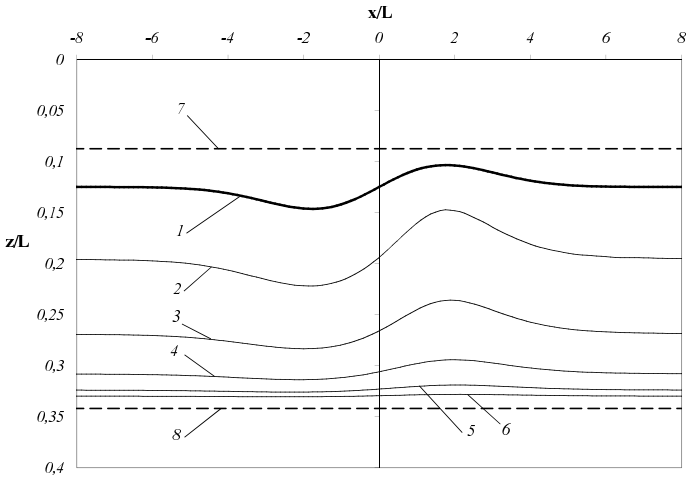

Figure 11: Evolution of the phase transition front for $\alpha = 0.03, \beta = 0.6, \overline{Z}_0 = 0.125$. The curves enumerated in correspondence with growing time; lines 7 and 8 correspond to the unstable and stable equilibria, respectively.

of the phase transition fronts are in some sense governed by bifurcation diagrams of the stationary fronts, namely, if the stable branch of the bifurcation curve exists for given parameters it serves as an attractor for moving fronts. If it doesn't exist (when we are to the right of the turning point) then the moving front tends to move upstairs and reaches the upper boundary of the layer at finite time.

The stability properties of small perturbations of the plane moving front of phase transition are also connected with the parameter domains of stability/instability St, Lo, S, U of stationary plane fronts, namely, the perturbations are subjected to either stability, or instability if the moving front locates in the respective domain. Note, that the boundaries of the domains St, Lo, S and U in the $(r, \overline{Z})$ plain are determined only by the quantity $r = \alpha/\beta$; i. e., either decrease or increase of the perturbations depends not on α and β themselves, but on their ratio. Each of these dimensionless parameters is proportional to g^{-1}, therefore the parameter r does not depend on gravity. Thus, the character of evolution of perturbations of the surface of phase transition fronts (but not the direction of the motion of the front as a whole) depends only on the processes of diffusion and filtration under action of the pressure gradient, but not on gravity.

We also study numerically the dynamics of finite localized perturbations. It is seen from Fig. 9 that such perturbations evolve according to the scenario of evolution of infinitesimal harmonic perturbations. The different speed of variation of amplitude of disturbances propagating up and down and also the increase of "effective" length of the disturbance would be referred to nonlinear effects.

In Fig. 10 growth of short-wave perturbations has an uncontrolled character. When the size of the mesh is modified the wave length of these perturbations and the rate of

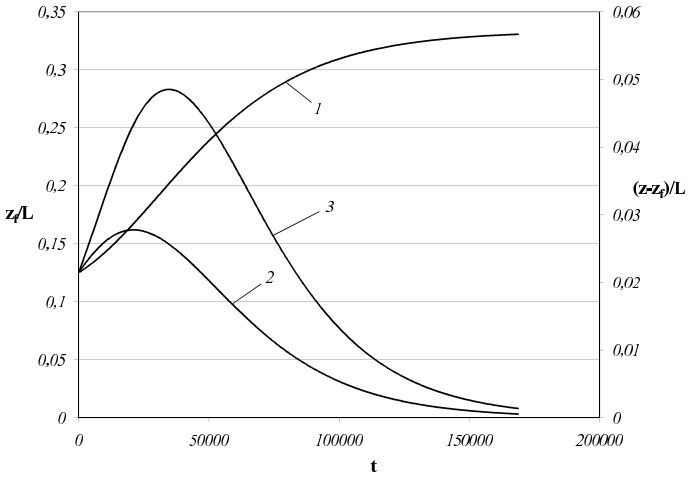

Figure 12: Dependence of the coordinate of the phase transition interface $\overline{Z}_a$ (line 1) and amplitude of perturbations (lines 2,3) on time; $\alpha = 0.03$, $\beta = 0.9$, $\overline{Z}_0 = 0.125$. Line 2 corresponds to the perturbation directed upstairs, and line 3 - downstairs.

growth of their amplitude will be different. This instability of numerical solution is the result of violation of the causality condition for very short perturbations. However, the process of damping of the long-wave perturbation can be correctly computed only until the amplitude of short-wave perturbations is much smaller than that one of long-wave perturbations. If the lower branch of the bifurcation curve entirely lies in the domain St, (lines 3 and 4 in Fig. 5) or at least the attracting equilibrium lies in the domain St (for line 5 in Fig. 5 it is a part of the lower branch, lying to the left from point D), then short-wave perturbations are not developing as the front moves; in this case they do not prevent the computation.

Fig. 12 shows that the nonlinearity becomes apparent in the different growth of perturbations propagating upstairs and downstairs: the perturbation directed to the stable equilibrium position grows slower but decreases faster. In this example all points of the perturbed front lie strictly between the equilibria, but in Fig. 13 it is not so. From this figure it is seen that scenarios of evolution obtained from linear analysis for small perturbations are reliable only when the entire front lies in the domains St and Lo.

Short-wave instability develops stronger the shorter the perturbation. Therefore, there exist the very short waves in the domain U (higher than line 9 in Fig. 13), such that the horizontal size of a section of the front above line 9 is much longer than these perturbations. So it can be treated as the base flow in the U, and the perturbations of this section can grow infinitely fast. Development of uncontrolled short-wave perturbations particularly visible on lines 5 and 6. In other words, if we want the numerical modeling in the case when the front doesn't lie entirely in the domains St or Lo to give the reliable picture of development of perturbations the governing equations have to be changed.

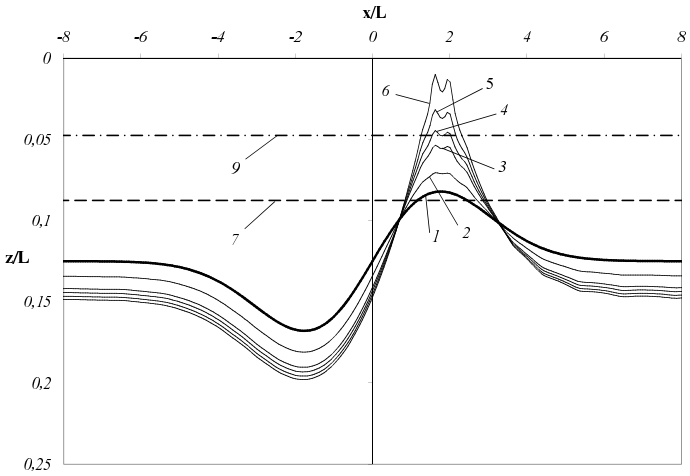

Figure 13: Evolution of the phase transition front for $\alpha = 0.03, \beta = 0.9, \overline{Z}_0 = 0.125$. The curves enumerated in correspondence with growing time, line 7 corresponds to the unstable equilibrium position, and line 9 to the boundary of the domain of instability U.

In the paper we find that the configuration in question is always stable for wettable media, and it can be unstable for the non-wettable one. Usually, the water is the wetting phase in the majority of air-water-natural rock systems. Yet, if the permeability rock contains coal particles, (for example, it can occur in mines) then such a media is non-wetting one for the water. Moreover, for artificial underground constructions one uses the hydrophobic cement, which is the non-wettable medium because of special additives.

Acknowledgement. This work was carried out under financial support by Russian Foundation of Basic Research, projects No 14-01-00466 and 13-01-12047.

References

[1] Kolabin, G. V., Dyad'kin, Yu. V., Arens, V. Zh. (1988) *Thermophysical Aspects of Development of Underground Resourses*, Nedra: Leningrad, (in Russian).

[2] Schubert, G., Straus, J.M (1980) Gravitational stability of water over steam in vapour-dominated geothermal system, *J. Geoph. Res.*, **85**, 6505–6512.

[3] Tsypkin, G., Il'ichev, A. (2004) Gravitational stability of the interface in water over steam geothermal reservoirs. *Transport in porous media*, **55**, 183–199.

[4] Il'ichev A.T., Tsypkin G.G. (2005) Transition to instability of the interface in geothermal systems. *European Journal of Mech. B/Fluids*, **24**, 491–501.

[5] Khan Z.H., Pritchard D. (2013) Liquid-vapour fronts in a porous media: Multiplicity and stability of front positions. *Int. J. Heat Mass Transfer*, **61**, 1–17.

[6] Il'ichev A.T., Tsypkin G.G. (2008) Catastrophic transition to instability of evaporation front in a porous medium, *European Journal of Mech. B/Fluids*, **27**, 665–677.

[7] Il'ichev A.T., Tsypkin G.G, (2008) Instabilities of uniform filtration flows with phase transition, *J. Exp. Theor. Phys.*, **107:4**, 699–711.

[8] Il'ichev A.T., Shargatov V.A. (2013) Dynamics of water evaporation fronts, *Computational Mathematics and Mathematical Physics*, **53**, 1350–1370.

[9] Kolmogorov, A. Petrovsky, I. Piscounov, N. (1937) Etude de'équation de la diffision avec croissance de la quantité de matière et son application à un problème biologique. *Moscow Univ Math Bull.*, **1**, 1–25.

[10] D. R. Lide, *CRC Handbook of Chemistry and Physics*, Boca-Raton: New-York, Washington, (2001-2002).

[11] Tsypkin G.G., Woods A.W. (2004) Vapour extraction from a water saturated geothermal reservoir, *Journal of Fluid Mechanics*, **506**, 315–330.

[12] Vukalovitch, M. P. (1955) *Thermodynamic Properties of Water and Water Vapor*, Mashgiz: Moscow, (in Russian).

[13] V. Yu. Lyapidevskii and V. M. Teshukov, *Mathematical Models of Propagation of Long Waves in an Inhomogeneous Fluid*. Novosibirsk, Russian Federation: Publishing House of the Siberian Branch of RAS, 2000 (in Russian).